

# Chromatin Shapes the Mitotic Spindle

Ana Dinarina,<sup>1,4</sup> Céline Pugieux,<sup>1,4</sup> Maria Mora Corral,<sup>1</sup> Martin Loose,<sup>1,5</sup> Joachim Spatz,<sup>2,3</sup> Eric Karsenti,<sup>1</sup> and François Nédélec<sup>1,\*</sup>

<sup>1</sup>Cell Biology and Biophysics Unit, European Molecular Biology Laboratory, Heidelberg D-69117, Germany

<sup>2</sup>Department of Biophysical Chemistry, University of Heidelberg, Heidelberg D-69120, Germany

<sup>3</sup>MPI for Metals Research, Heisenbergstr. 3, 70569 Stuttgart, Germany

<sup>4</sup>These authors contributed equally to this work

<sup>5</sup>Present address: Biophysics, BIOTEC, Technische Universität Dresden, Tatzberg 47-51, Dresden 01307, Germany

\*Correspondence: nedelec@embl.de

DOI 10.1016/j.cell.2009.05.027

## SUMMARY

In animal and plant cells, mitotic chromatin locally generates microtubules that self-organize into a mitotic spindle, and its dimensions and bipolar symmetry are essential for accurate chromosome segregation. By immobilizing microscopic chromatin-coated beads on slide surfaces using a micro-printing technique, we have examined the effect of chromatin on the dimensions and symmetry of spindles in *Xenopus laevis* cytoplasmic extracts. While circular spots with diameters around 14–18  $\mu\text{m}$  trigger bipolar spindle formation, larger spots generate an incorrect number of poles. We also examined lines of chromatin with various dimensions. Their length determined the number of poles that formed, with a  $6 \times 18 \mu\text{m}$  rectangular patch generating normal spindle morphology. Around longer lines, multiple poles formed and the structures were disorganized. While lines thinner than 10  $\mu\text{m}$  generated symmetric structures, thicker lines induced the formation of asymmetric structures where all microtubules are on the same side of the line. Our results show that chromatin defines spindle shape and orientation.

For a video summary of this article, see the [PaperFlick](#) file available with the online [Supplemental Data](#).

## INTRODUCTION

The mitotic spindle performs an essential task during eukaryotic cell division: the segregation of sister chromatids. This function implies the establishment of a plane of symmetry, which is materialized by the metaphase plate, orthogonal to the spindle axis and on which the chromosomes are positioned before being separated. During anaphase, chromosomes are segregated by microtubules that bind to sister kinetochores, located on opposite sides of each chromosome. This requires the existence of two overlapping and connected arrays of antiparallel microtubules, capable of resisting inward directed forces produced by the pulling forces of the kinetochore microtubules.

Two pathways of spindle assembly have been identified, the centrosomal and the chromatin pathway (Walczak and Heald, 2008). They are independent and complementary and cells

may rely on one or both pathways to assemble a spindle. For example, two centrosomes and kinetochore pairs positioned back-to-back on sister chromatids may be sufficient to form a spindle in the small yeast cell (Winey et al., 1995). In contrast, in large cytoplasmic volumes such as in *Xenopus laevis* egg extracts, spindles can assemble in the absence of kinetochores and centrosomes (Heald et al., 1996). In this system, microtubules are generated near chromatin and organized into a bipolar spindle by associated proteins, hence the term “chromatin pathway” (also known as acentrosomal). Understanding this pathway is of major importance because it is found in higher eukaryotes, including frogs, green monkeys (Khodjakov et al., 2000), *Drosophila* S2 cells (Goshima et al., 2008; Mahoney et al., 2006), *Drosophila* oocytes (Matthies et al., 1996), mouse oocytes (Schuh and Ellenberg, 2007), human cells (Bird and Hyman, 2008), and plants (Lloyd and Chan, 2006).

Although the enzymatic mechanism by which the chromatin pathway controls local microtubule growth has been partly resolved (Walczak and Heald, 2008), the overall effects of chromatin on spindle size and symmetry properties have not been examined. This issue has been addressed using spindles assembled around artificial chromosomes in *X. laevis* egg extracts, but there was no method to create chromatin in a defined shape. The other challenge was to obtain statistically meaningful data on the relationship between chromatin mass and spindle properties. Only one study has examined the effect of chromatin geometry on spindle morphology (Gaetz et al., 2006), but the method was limited in the variety of chromatin patterns that could be tested.

We have devised a new method to control both the size and geometry of chromatin patterns and to study their impact on the morphology of mitotic spindles. We were also able to capture time-lapse movies of spindle assembly, including the initial nucleation phase. We found that chromatin size and geometry play a fundamental role in the determination of spindle size and define the characteristic symmetries of the structure.

## RESULTS

### Spindles Self-Organize on Chromatin-Coated Immobilized Beads

It has long been known that large DNA plasmids (about 10 kb or more) could trigger spindle assembly when injected into *X. laevis* eggs (Karsenti et al., 1984). However, the exact quantity of chromatin required to make a spindle remained unknown. For

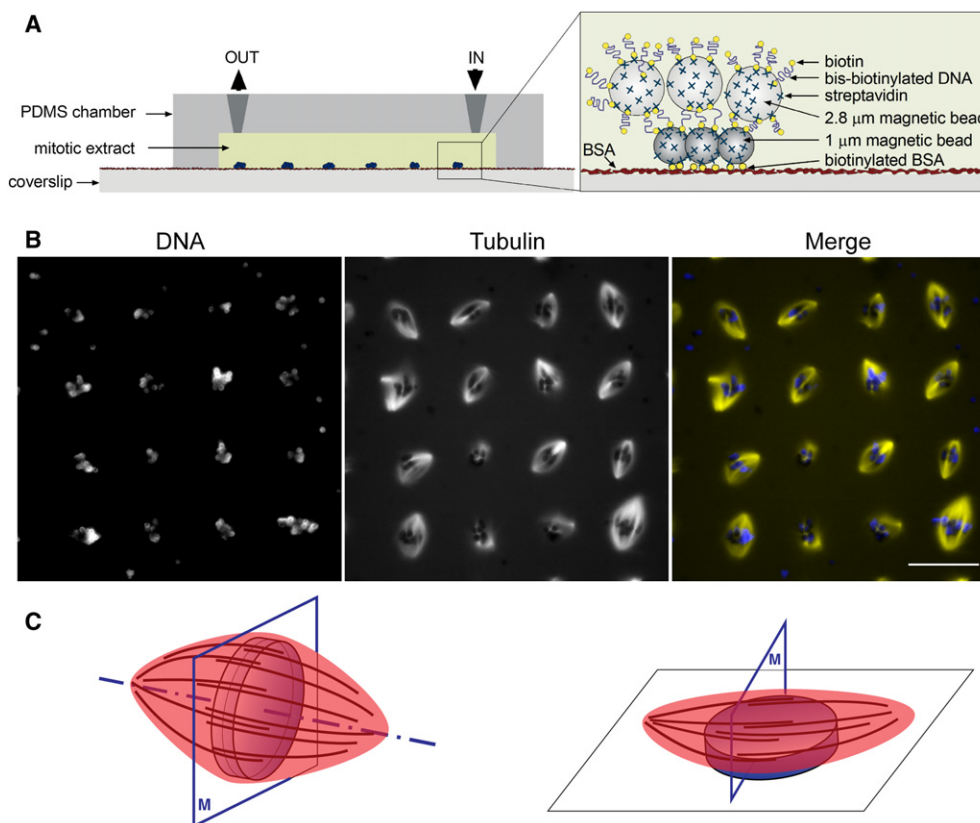


**Figure 1. Spindle Arrays**

(A) Experimental setup. Biotinylated BSA is first printed on a glass coverslip following a lithographic micropattern. A layered structure is then assembled with 1  $\mu\text{m}$  streptavidin-coated paramagnetic beads and chromatinized bis-biotinylated plasmid DNA-coated 2.8  $\mu\text{m}$  beads. The chromatin pattern is sealed by a PDMS flow-through chamber and incubated with fresh mitotic *X. laevis* egg extract.

(B) Spindle organization around chromatin spots. (Left) Hoechst DNA staining. The spots of diameter  $\sim 15 \mu\text{m}$  are arranged  $\sim 37 \mu\text{m}$  edge-to-edge. (Middle) Cy3-labeled tubulin after 60 min incubation with *X. laevis* egg extracts. Scale bar, 50  $\mu\text{m}$ .

(C) (Left) A theoretical metaphase spindle, having mirror symmetry with respect to the metaphase plate (M) and rotational symmetry around an axis perpendicular to it. (Right) Spindles formed around a chromatin spot immobilized on the glass surface. Rotational symmetry is lost, but mirror symmetry is retained.

example, spindles did not form in *X. laevis* egg extracts around DNA directly attached to a glass substrate (Dogterom et al., 1996). On the other hand, DNA beads densely coated with plasmid DNA did induce spindle assembly in extracts (Gaetz et al., 2006; Heald et al., 1996; Maresca and Heald, 2006). Here, we have used beads of diameter 2.8  $\mu\text{m}$ , coated with DNA, on which chromatin was preassembled in an interphase extract. The beads were then immobilized on patterns defined by lithography on a surface (see Experimental Procedures). These bead patterns were subsequently incubated with mitotic *X. laevis* egg extract in a flow-through chamber (Figure 1A). Microtubule nucleation and organization were monitored using confocal fluorescence microscopy under temperature-controlled conditions. This method offered key advantages over previous approaches, namely the possibility to set the shape of chromatin, the ability to follow spindle assembly as a function of time, and the imaging of a large number of spindles in each experiment.

To demonstrate the functionality of the assay, chromatin beads coated with 0.5  $\mu\text{g}$  of DNA/bead were first immobilized

on a pattern of circular spots of diameter 15  $\mu\text{m}$  (Figure 1B). Microtubules appeared on more than 95% of the spots within 5–10 min and matured into distinguishable structures within  $\sim 30$ –60 min (Figure 1B and see Movie S1 available online). On this pattern, 65% of the spots generated bipolar spindles (Figure S1), which is consistent with the incidence of spindles observed for unattached beads (Heald et al., 1996). Where bipolar spindles did not form, we observed mostly monopolar or tripolar structures. The chromatin spots were parallel to the surface and represented chromatin plates that were rotated by  $90^\circ$  with respect to the microtubules (Figure 1C). Yet, the attachment of chromatin on the surface did not seem to affect the functional organization of the microtubules. Spindle dimensions were comparable to those formed around unattached beads or sperm nuclei (Heald et al., 1996). Movie S2 shows a typical surface spindle in 3D.

#### Chromatin Mass Affects Spindle Length Moderately

To measure the influence of chromatin mass on the spindles, the amount of DNA per bead was varied on a pattern containing

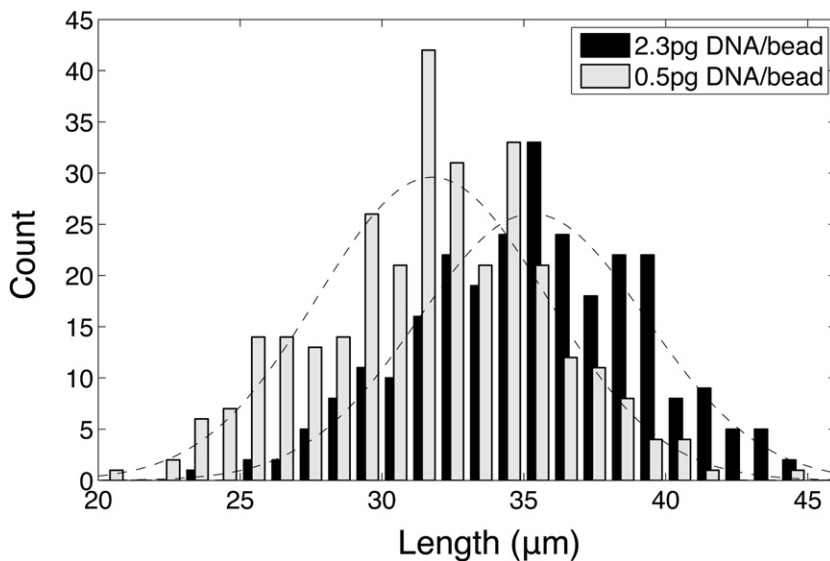


**Figure 2. Influence of Chromatin Mass on Spindle Length**

Spindles formed around circular spots of uniform size, as shown on Figure S1, with beads carrying either 0.5 or 2.3 pg of DNA. With 0.5 pg DNA/bead, lengths of 307 spindles were  $31.76 \pm 4.03 \mu\text{m}$  (mean and standard deviation) while with 2.3 pg DNA/bead, 268 spindles were  $35.30 \pm 4.01 \mu\text{m}$  long. The histograms have Gaussian profiles (dashed lines). Increasing the amount of DNA while keeping the printed area resulted in longer spindles.

spots of diameter  $15 \mu\text{m}$ . Spindle lengths were  $31.76 \pm 4.03 \mu\text{m}$  with 0.5 pg DNA/bead and  $35.30 \pm 4.01 \mu\text{m}$  with 2.3 pg DNA/bead (Figure 2). Thus the  $\sim 5$ -fold increase of DNA mass lengthened the spindles by  $\sim 10\%$ . This is significant but modest and hints that chromatin influences the cytoplasm through a surface effect rather than a volume or a mass effect. Indeed, DNA itself has no direct influence on microtubules. Chromatin contains enzymes such as RCC1 that activate Ran and downstream factors that promote microtubule assembly (Athale et al., 2008). In that scenario, only the outer surface of a dense chromatin mass is expected to activate Ran, and it is thus instructive to roughly estimate the chromatin surface in our assay. Assuming a density of 1, the thickness  $e$  of the chromatin layer on beads of radius  $R = 1.4 \mu\text{m}$  is  $\sim 20 \text{ nm}$  with 0.5 pg of DNA and  $\sim 100 \text{ nm}$  with 2.3 pg. The outer surface area  $S = 4\pi(R + e)^2$  changes from  $\sim 25$  to  $\sim 28 \mu\text{m}^2$ , also a moderate increase of 11%. While this calculation does not account for the real reaction-diffusion dynamics taking place around a set of beads, it may explain the modest influence of the amount of DNA per beads. Because chromatin mass weakly affects the spindle, we focused further efforts on the spatial configuration of chromatin, always using 0.5 pg of DNA per beads.

### Chromatin Size Affects Spindle Dimensions and Symmetry

When we used a pattern consisting of round chromatin spots of various diameters (Figure 3A), bipolar spindles formed preferentially around  $14\text{--}18 \mu\text{m}$  spots (Figure 3B). Smaller spots produced a low percentage of bipolar spindles, most of them failing to initiate a robust structure. Spots larger than  $18 \mu\text{m}$  produced a high proportion of multipolar structures. Thus, chromatin spot diameter was strongly correlated with the symmetry of microtubule organization.

We then measured the length (pole-to-pole distance) and width of those structures that were bipolar, as a function of spot diameter. The length of the spindles increased linearly with spot diameter, such that for any chromatin spot size, the pole tips

were always positioned  $\sim 10 \mu\text{m}$  away from the edge of the spots (Figure 3C). Spindle width also increased linearly with spot size until  $24 \mu\text{m}$  (Figure 3C). The excess of spindle width over spot diameter corresponds to flanking microtubule bundles connecting the two poles around chromatin. Their thickness decreased gradually to almost zero for a chromatin spot diameter of  $24 \mu\text{m}$ . It is interesting that this corresponds to the size at which spindles become multipolar. It suggests that bipolarity relies on the width of the flanking bundles, but another possibility is that it depends on the pole-to-pole distance.

### Microtubule Polymer Mass Is Proportional to Bead Count and Constantly Turned Over

Metaphase corresponds to a steady state, where continuous microtubule loss in the spindle is compensated by the constant nucleation of microtubules by chromatin (Desai and Mitchison, 1997). In the spindle arrays, assembly initially overcomes disassembly and a steady state is established as the two rates equalize. This happens either because assembly decreases or because disassembly increases. The simplest scenario is that disassembly is proportional to the polymer mass in the structure, which occurs if microtubules have a finite lifetime. To examine this issue further, we quantified the total amount of microtubule polymer, by summing the intensity of Cy3-tubulin in a disc of  $43 \mu\text{m}$  radius centered on each chromatin spot. The background fluorescence level corresponding to free tubulin was subtracted, to define the total “polymer mass” in the disc. The results are presented as a function of time in Figure 3D, for the spots shown on Figure 3A (similar results were obtained for other experiments). Large spots nucleated microtubules earlier and faster than smaller spots. On large spots, polymer mass overshoot before decreasing back to a plateau after 20–30 min. We also examined the total amount of microtubule polymer assembled between 20 and 40 min, as a function of chromatin bead count for each spot. Polymer mass increased linearly with the bead number (Figure 3E) beyond a threshold of approximately four beads (2 pg of DNA). Below this threshold (indicated by red dots on Figure 3E), the spots nucleated only a few microtubules.

These results show that there is a correlation between dimensions of chromatin, spindle size, and steady-state polymer mass. To examine which mechanisms could be implicated, we considered three dynamic models in which the total polymer mass in

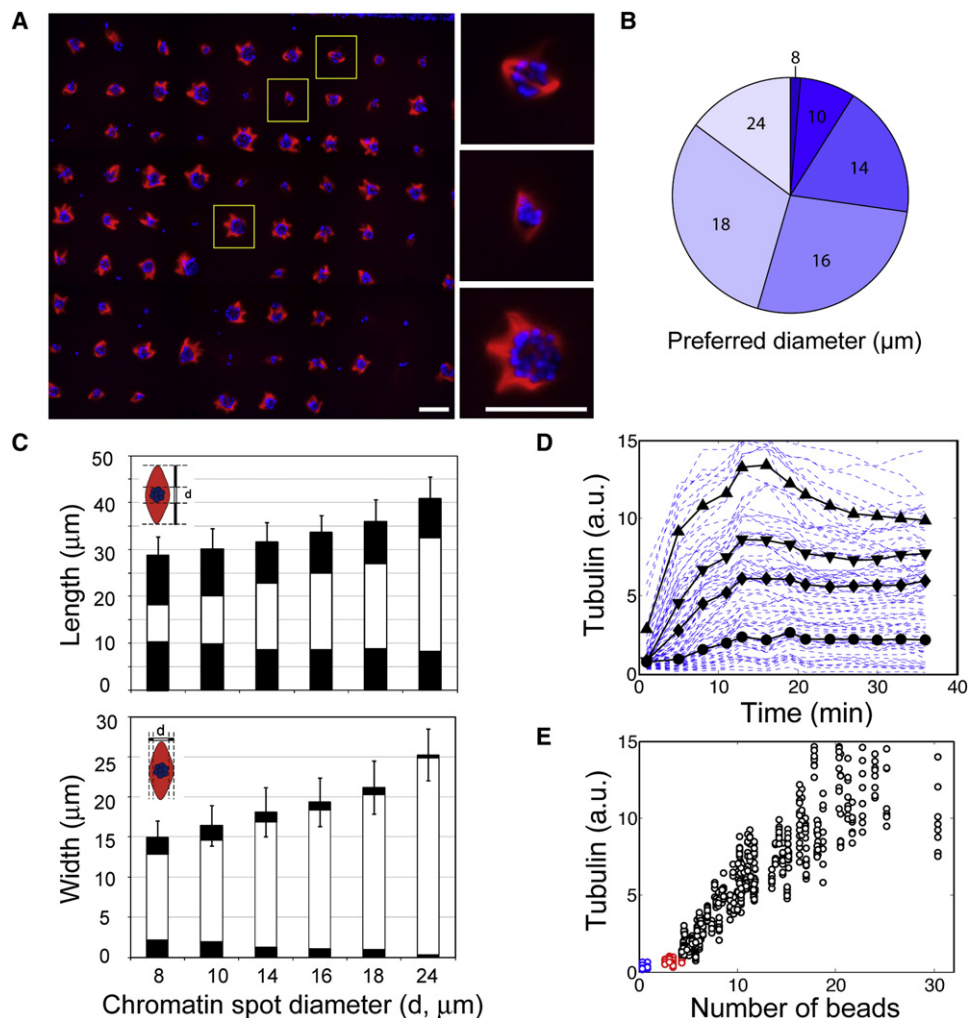


**Figure 3. Influence of Chromatin Geometry on Spindles**

(A) Structures assembled on chromatin spots of diameters 8, 10, 14, 16, 18, and 24 μm (separation of ~58 μm) with 0.5 pg DNA/bead. Red, tubulin; blue, chromatin. Scale bars, 50 μm.

(B) Distribution of spindles over the diameters of the chromatin spots on which they formed (290 bipolar symmetric structures from four independent experiments). An equal number of spots were considered for each category, such that this result reflects the relative bipolar rate as a function of chromatin size.

(C) Length and width of spindles with standard deviations. The total bar represents the dimension of the spindles and the central white portion represents the diameter of the spots. With spindle length, the remaining black portion is thus the distance from the pole to the chromatin edge.

(D) Polymer mass (background-subtracted total tubulin fluorescence) generated by chromatin spots, as a function of time (time zero corresponds to the onset of nucleation). Thin dashed lines indicate individual spots. Averages are shown in black for each category according to the number of beads: (●) 0-9 (average = 4.5), (◆) 10-12 (average = 10.8), (▼) 13-17 (average = 14.6), and (▲) 18-30 (average = 23.8). Standard deviations that are omitted here for clarity are indicated on Figure 4.

(E) Spindle mass at steady state, as a function of bead count. Spots lacking chromatin beads and spots without structures are shown in blue and red, respectively. Each dot on the graph corresponds to a single spot and a single time point (81 spots, eight time points between 20 and 40 min, from experiment shown in (A); Similar results are obtained for other experiments).

the structure is represented by a scalar  $m$ . In the first model, we assumed that (1) a quantity  $c$  of chromatin constantly generates  $g c$  polymer mass per minute, and (2) that the polymer has a finite life span  $\tau$ , due to dynamic instability of microtubules. However, the model failed to reproduce the observed overshoot (Figure 4A, left). We therefore built a second model in which microtubule disassembly involved an additional enzymatic activity ( $k$ ) that can be adjusted. Such a model is described by

$dm/dt = g c - k$  and  $dk/dt = m/\sigma - k/\tau$ , in which  $m$  is again the polymer mass and  $k$  the depolymerizing activity of the enzyme. As before, the quantity  $c$  of chromatin generates constantly  $g c$  polymer mass per minute. The polymer is destroyed by the activity  $k$ , which is in equilibrium with the polymer: a quantity  $m/\sigma$  binds per minute and remains bound (active) for a time  $\tau$  on average. This simple model fits the measurements with parameters  $\sigma = 36 \text{ min}^2$  and  $\tau = 5.3 \text{ min}$  (Figure 4A, center).

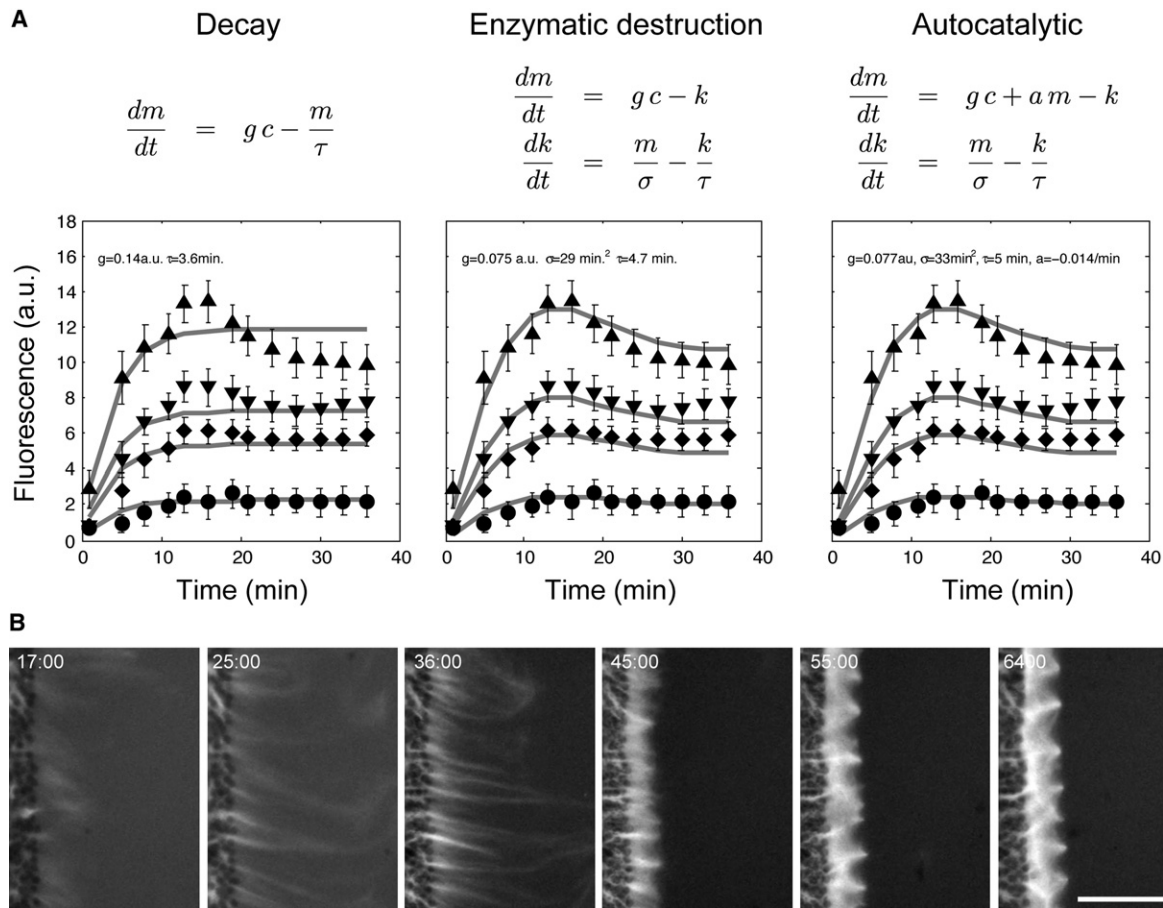


**Figure 4. Models of Polymer Generation**

(A) Fit by simple models of the time course of microtubule assembly around round spots of various chromatin contents. The four categories are extracted from Figure 3D, together with the average measured number of beads  $c$  ( $\bullet = 4.5$ ,  $\blacklozenge = 10.8$ ,  $\blacktriangledown = 14.6$ , and  $\blacktriangle = 23.8$ ). The error bars indicate  $\pm 1/2$  standard deviation. For each model, the parameters  $g$ ,  $\sigma$ ,  $\tau$ , and  $a$  are obtained using a simplex optimization method (Matlab's function `fminsearch`) to minimize the squared deviation from the experimental data. (left) Chromatin generates microtubules, which depolymerize spontaneously. (middle) Chromatin generates microtubules, which recruit a depolymerizing activity. (right) In addition to these processes, microtubules can generate other microtubules in an autocatalytic manner (additional term  $+am$ ). Since the polymer mass is measured using fluorescence, it is in arbitrary units, and the parameters  $g$  or the values of  $k$  are not directly interpretable. However,  $\sigma$  and  $\tau$  are in units of minutes and can be interpreted as follows: while  $\tau$  is the unbinding rate of the activity,  $\sigma$  encapsulates both the binding rate and the time scale of the depolymerization activity.

(B) Initial phase of microtubule organization from chromatin. Microtubules (which may be bundled) extend up to  $50 \mu\text{m}$  away from the chromatin edge. Scale bar,  $50 \mu\text{m}$ . The time (min:s) indicated is taken from the start of incubation at  $20^\circ\text{C}$  in the microscope chamber.

The polymer mass overshoots because the depolymerization activity takes some time to affect the polymer. This is supported by the observation that microtubules nucleated close to chromatin can extend initially up to  $50 \mu\text{m}$  away before being trimmed back to fit in a spindle (Figure 4B and Movie S1). The overshoot in polymer mass thus corresponds to an overshoot in microtubule length.

It has been proposed that during spindle assembly, microtubules are nucleated along preformed microtubules, thereby establishing an autocatalytic loop (Mahoney et al., 2006). To examine whether this would improve the fit of the model to the experimental results, we added a term  $am$  in the first equation. This offered the possibility to make microtubules exist for a finite time ( $a < 0$ ) or to generate an autocatalytic production of microtubules ( $a > 0$ ). Yet, this did not significantly improve the quality of

the fit (Figure 4A, right). Either these effects are not important for polymer mass determination or their respective contributions cancel out precisely. In an autocatalytic mechanism, the polymer mass should initially increase exponentially (Clausen and Ribbeck, 2007), but this was not detectable around chromatin spots in our experiments.

Our quantifications of the polymer mass included all structures irrespective of their symmetry. Since bipolar spindles formed around a preferred spot diameter (Figure 3B), their polymer mass must also have a preferred range. Furthermore, polymer mass is a combination between the number of microtubules and their length distribution, but our analysis does not allow to sort these two contributions apart. Nevertheless, above a threshold, the steady-state polymer mass is proportional to the amount of chromatin beads. The assembly dynamics further

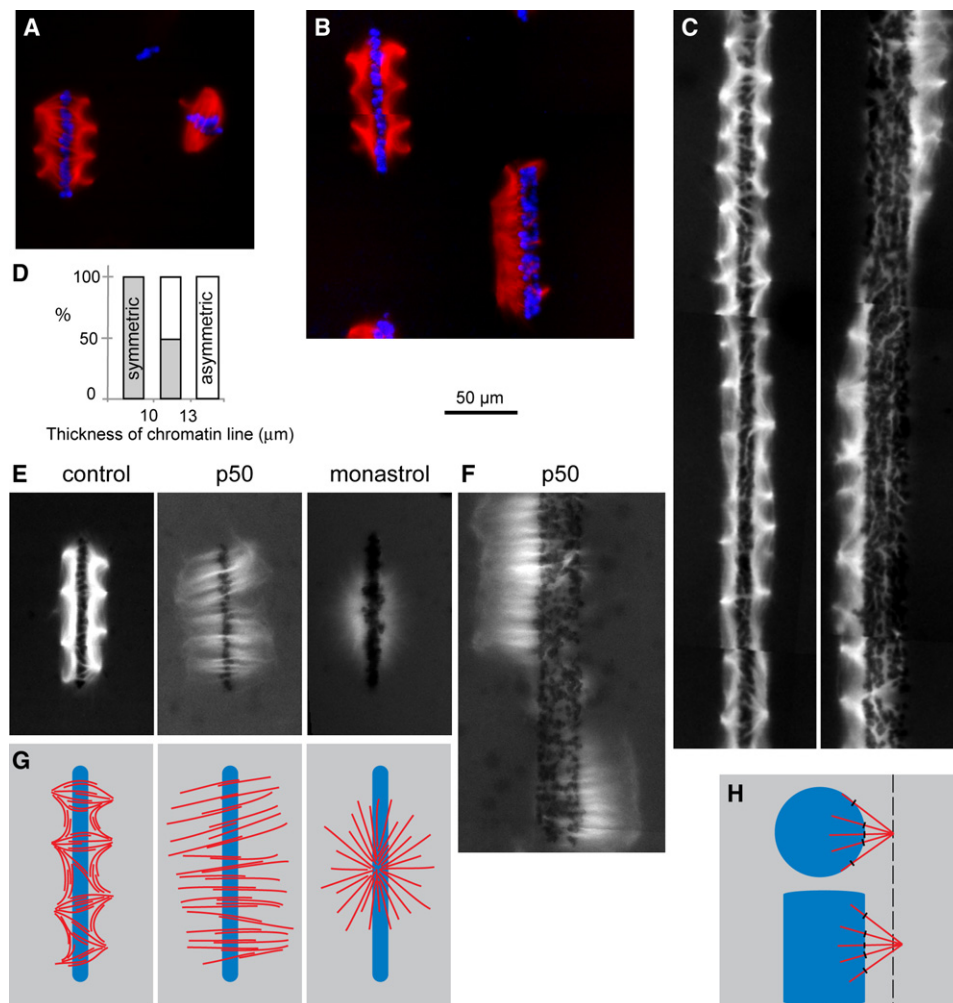


**Figure 5. Chromatin Lines**

(A) Structures assembled on long (100  $\mu\text{m}$ ) and short (20  $\mu\text{m}$ ) chromatin lines.

(B) Chromatin lines of thicknesses  $\sim 7 \mu\text{m}$  and  $\sim 15 \mu\text{m}$ , respectively.

(C) 450  $\mu\text{m}$  long chromatin line with thickness of 10  $\mu\text{m}$  (left) or 30  $\mu\text{m}$  (right).

(D) Symmetry of the steady-state structures as a function of line width ( $n = 78$  structures from two experiments).

(E) Microtubule organization on a 100- $\mu\text{m}$ -long thin (width  $< 10 \mu\text{m}$ ) chromatin line in control extract and extract containing either 100  $\mu\text{M}$  monastrol (an inhibitor of Eg5) or 1  $\text{mg ml}^{-1}$  p50 (an inhibitor of dynein).

(F) Microtubule organization on a 30  $\mu\text{m}$ -thick chromatin line in extracts containing p50. Red, tubulin; blue, chromatin. All pictures are shown with the same magnification; scale bar, 50  $\mu\text{m}$ .

(G) Microtubule directions in the structures shown in (E).

(H) A pole should be more distant from a straight edge than from a convex one if its position is determined by overlaps between microtubules and chromatin.

indicate that chromatin is steadily active and that microtubules recruit their own depolymerizing activity.

#### Length of Chromatin Line Determines Number of Spindle Poles

Results so far indicated that for a given geometry (a flat disk), chromatin size could determine quantitatively both the dimensions and symmetry of microtubule structures. In a given species, the spindle components must be such that a bipolar spindle assembles around a defined chromatin size. Our results showed that indeed there is a well-defined range over which proper bipolar structures assemble. However, while the circular

geometry matches roughly the pool of chromosomes in prophase, in metaphase they occupy a cylindrical volume. We therefore investigated how microtubules would self-organize around lines of chromatin mimicking a preestablished metaphase plate.

A  $6 \times 18 \mu\text{m}$  rectangular patch best matched the configuration of chromatin in a *X. laevis* metaphase spindle and indeed generated normal spindle morphology (Movie S4). As shown in Figure 5A, we found that only one bipolar spindle forms orthogonal to the line axis when the chromatin lines are shorter than  $\sim 30 \mu\text{m}$ . Yet, for longer chromatin lines, the structures formed had multiple poles on both sides (Figures 5A–5C and 5E,

left; Figure S2 and Movie S3). The distance between neighboring poles on the same side of the chromatin line were  $23.11 \pm 6.33 \mu\text{m}$  ( $n = 300$ ), which is comparable to the width of sperm-head spindles. This was in stark contrast with the previous findings that only one spindle would form per line, up to  $\sim 100 \mu\text{m}$  in length (Gaetz et al., 2006). Poles on opposite sides of the line seemed to interact but were not necessarily in register (see for example Figure 5C). Interestingly, pole microtubules also interacted with adjacent poles on the same side of the chromatin line, forming antiparallel overlaps running parallel to the chromatin line (Figures 5E and 5G). This implies that these structures cannot be functional, since antiparallel overlaps should be perpendicular to the metaphase plate for proper chromosome segregation. In short, a functionally organized spindle will form on a chromatin line only up to a certain length.

The distance between the poles and the nearest edge of the chromatin was  $14.6 \pm 3 \mu\text{m}$  for a line thickness of  $8 \mu\text{m}$ ,  $16.1 \pm 2.6 \mu\text{m}$  for  $15 \mu\text{m}$ , and  $14.9 \pm 2.4 \mu\text{m}$  for  $23 \mu\text{m}$  (data collected over 100 poles belonging to symmetric structures). Thus the poles remained roughly  $15 \mu\text{m}$  away from the edge of the chromatin lines, for all thicknesses tested. This result is analogous to that obtained on circular spots of different diameters, where the distance between the chromatin edge and the pole was  $\sim 10 \mu\text{m}$  (Figure 5H).

### Thickness of Chromatin Line Determines Symmetry

Lengthening the line disorganized the structures and widening the line had a surprising effect on spindle symmetry. While microtubule organization was initially symmetric for thin and thick lines, the two-fold symmetry was lost for lines thicker than  $10\text{--}13 \mu\text{m}$  such that microtubules were eventually localized only on one side of the lines (Figures 5B–5D). The asymmetric organization is naturally inoperative. Movie S5 illustrates the surprising dynamics of asymmetric structures around thick lines. They sometimes flipped together from one side of the chromatin line to the other within  $\sim 15$  min. In short, a symmetric structure will form only below a certain chromatin thickness and the system is unstable beyond that thickness.

Additional experiments were performed to characterize the asymmetric structures formed on wide chromatin lines. First, speckle imaging (Waterman-Storer et al., 1998) was used to measure the motion of microtubules. They globally move at a speed of  $\sim 2.85 \pm 0.95 \mu\text{m}/\text{min}$  (data from five structures) away from the chromatin (see example on Figure S3 and Movie S6). The flux is similar in speed than in bipolar spindles (Miyamoto et al., 2004), but it only occurs in one direction. We do not exclude, however, that the structure may contain a region of antiparallel flux, since the chromatin beads mask the speckles in our imaging setup. Next, 0.5% hexylene glycol was added to increase the average length of microtubules (Mitchison et al., 2005). These conditions increased the length of sperm-head-generated spindles by 26% (data not shown) and increased the width of chromatin necessary to render microtubule organization asymmetric (Figure S4). Specifically,  $15 \mu\text{m}$  wide lines generated asymmetric structures in untreated extracts but symmetric ones in the presence of hexylene glycol. This can mean that the transition occurs for a certain ratio of chromatin width to spindle/microtubule length.

For the system to fold to one side of the line, microtubules on opposite sides of a line must be able to interact. To estimate the range of this remaining interaction, the line thickness was increased even more, and at  $\sim 65 \mu\text{m}$  microtubules are present on both sides (Figure S2). This corresponds to a second transition, where the system regains symmetry because the distance between the two sides outranges all interactions, leading to the formation of independent microtubule structures. Such disconnected structures are also inoperative.

### Thick Chromatin Lines Prevent Pole Interactions, Mediated by Eg5 and Dynein

The molecular motors dynein and Eg5 are responsible for two primary forces driving microtubule organization in this system (Wittmann et al., 2001). Dynein creates a pole traction force, responsible for the focusing of microtubules into a pole or for the fusion of several poles during spindle assembly (Gatlin et al., 2009). The slow plus end-directed motor Eg5 creates an antiparallel interaction force, which is able to crosslink microtubules (Kapitein et al., 2008; Valentine et al., 2006). It is thought to push poles apart when they establish direct antiparallel microtubule overlaps.

The folding observed on thick lines could in fact be caused by dynein because it creates an attractive force that tends to fuse poles. To test this idea, we assembled spindles on chromatin lines, in the presence of p50/dynamitin, which disrupts the dynein complexes (Echeverri et al., 1996). As expected (Walczak et al., 1998), this prevented the formation of poles (Figure S1). On thin chromatin lines, this generated a symmetric brush of microtubules perfectly orthogonal to the chromatin line axis, extending symmetrically on both sides of the line (Figures 5E and 5G). In principle, such a structure could segregate chromosomes because it has a clean bipolar symmetry. On thick chromatin lines, inhibition of dynein activity did not restore bipolarity: microtubule brushes formed again perfectly orthogonal to the chromatin line, but they were asymmetric (Figure 5F). This indicated that (1) dynein complexes are not the cause of the asymmetric collapse and (2) the collapse is most likely caused by an oversized chromatin that prevents proper antiparallel interactions mediated by the motor Eg5.

Total inhibition of Eg5 by monastrol (Mayer et al., 1999) led to complete destruction of bipolarity and the formation of large asters (Figures 5E, 5G, and S1). The focal point of the aster was located above the chromatin line (Figure 5E). By observing the dynamics of assembly of those asters over a  $100 \mu\text{m}$  long chromatin line we discovered that microtubules were nucleated over the entire chromatin surface within 5 min, which was followed by their organization into a single large aster over another  $\sim 25$  min time span. Once formed, the poles moved along the chromatin lines and microtubules seemed to repeatedly assemble away from the aster, before being reabsorbed in it (Movie S7). In other words, when microtubules are nucleated along the chromatin line, in the absence of Eg5, dynein pulls them together into asters. On very long lines, the center-to-center distance between two asters was  $131 \pm 55 \mu\text{m}$  (mean and standard deviation, 24 measurements). This should correspond to the maximum range of the pole traction force presumably mediated by dynein along a chromatin line.

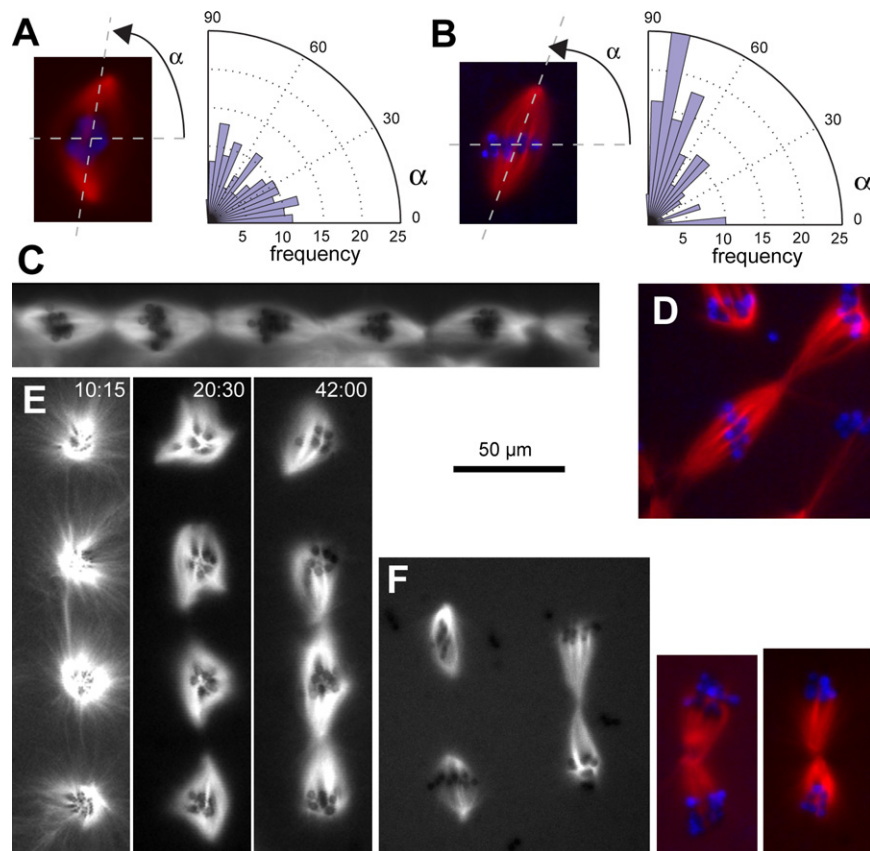


**Figure 6. Interacting Structures**

(A) Angular distribution of spindles formed on round chromatin spots (diameter of  $\sim 15 \mu\text{m}$ ) and (B) on lines (length of  $\sim 19 \mu\text{m}$ ). Each diagram represents 150 spindles from three experiments. (C) String of spindles interacting over aligned chromatin spots. (D) Spindle formed on a short chromatin line tilted by pole traction forces. (E) Time course showing the establishment of an interactive structure between three chromatin spots (min/s). (F) Examples of interacting and noninteracting structures, generated by pairs of chromatin spots. Scale bar,  $50 \mu\text{m}$ .

producing forces strong enough to rotate the structures. The balance between the chromatin effect (orthogonality) and the pole traction force (focusing of the pole) can be manipulated. For example, a spindle formed on a short chromatin line can be forced to adopt a permanent angle with respect to the chromatin, by placing other spindles sideways (Figure 6D). Here, the spindle must choose between the orthogonality to the chromatin line or the pole tractions. This example shows the dominance of the pole tractions over the chromatin-driven orientation in our assay.

### Pulling Forces Orient the Spindle

Circular chromatin spots did not provide any orientation clue since the spindles formed with their pole-to-pole axis parallel to the surface. The formation of a spindle around such a spot is thus a symmetry-breaking event in which the rotational symmetry is reduced to mirror symmetry (Figure 1C, right). It is expected to occur in a random direction, which is confirmed by the measurements (Figure 6A). In contrast,  $6 \times 18 \mu\text{m}$  chromatin patches are not rotationally symmetric and generated spindles preferentially perpendicular to their main axis (Figure 6B). Nevertheless, spindles exhibited surprising rotational motions. In Movie S4, for example, the pole-to-pole orientation varied over time by  $\pm 50^\circ$ , even though bundles of microtubules that pass between the beads bend in a “S” configuration, resisting misalignment. Thus while chromatin tends to orient microtubules perpendicular to it, on short lines a spindle could still wobble. For longer lines in the presence of p50, microtubules are well aligned and perpendicular to the chromatin (Figure 5F).

When two spindles in an extract are brought into contact, they normally fuse, such that eventually all chromatin forms a single metaphase plate (Gatlin et al., 2009). In our system, when chromatin spots were printed  $\sim 30 \mu\text{m}$  apart (edge-to-edge distance), spindles interacted but could not fuse because the chromatin was immobilized. They were nevertheless still free to mutually align each other (Figure 6C), showing that pole-to-pole interactions can orient spindles. Most probably, microtubules (which are sometimes visible) connected the two spindle poles,

Pole traction and antiparallel interaction can also be played against each other. For example, we observed a surprising loss of symmetry for the two end structures in a string of spindles (Figure 6E). Two bipolar spindles have four poles in total if they do not fuse (Figure 6F, left). However, when they interact, they form a “butterfly” motif with only one central pole (Figure 6F, right). Surprisingly, the distal poles have vanished as a consequence of the pole fusion. This shows that the pole traction force can destroy the antiparallel microtubule overlaps. Although this configuration was not tested, the fact that pole tractions should dominate antiparallel interactions has been anticipated theoretically (Burbank et al., 2007). In addition, the butterfly motifs show that the pole tractions do not usually pull off the microtubules from the chromatin, although exceptions were seen occasionally (Movie S1, middle top). This can be understood if microtubules are continuously generated by chromatin, but it could also be explained by other chromatin effects, such as the properties of chromokinesins (Bringmann et al., 2004). In the presence of p50, spindles do not align and interactive motifs are not observed, confirming that dynein is implicated in the pole traction (Figure S5) as recently showed (Gatlin et al., 2009).

In summary, chromatin effects can orient the microtubules orthogonal to the chromatin axis. The present competing configurations demonstrate that pole traction forces (dynein mediated) have an even stronger influence in determining the orientation of the microtubules. However, in vivo the two effects are not competing because the chromosomes are free to move and

rotate. Thus the spindle axis can orient within the cell and chromosomes can be oriented within the spindle.

## DISCUSSION

By printing chromatin beads in different configurations we uncovered new properties of spindle assembly. Varying the mass of DNA at constant geometry had a noticeable but weak effect on spindle length. On the contrary, varying the geometry of the area over which chromatin beads were immobilized influenced the system directly. For instance, the spindle poles remained  $\sim 15 \mu\text{m}$  away from straight edges and  $\sim 10 \mu\text{m}$  away from curved edges. The fact that poles are closer to curved edges is expected if the position of the pole is correlated with the overlapping of microtubules and chromatin (Figure 5H). However, it is currently unclear what defines the pole-to-edge distance. Dynein/Eg5-mediated forces and the local nucleation of microtubules and stabilization by chromatin (Athale et al., 2008) may certainly play a role. Chromatin also interacts with microtubules via chromokinesins such as Xkid and Xklp1 (Antonio et al., 2000; Bringmann et al., 2004; Tokai-Nishizumi et al., 2005). The positioning of the poles relative to chromatin edge can potentially be consistent with these diverse components, which need to be tested through mathematical modeling (Burbank et al., 2007). This is important to eventually understand what determines the spindle length.

While the pole-to-edge distances was  $\sim 15$  and  $10 \mu\text{m}$  for straight and curved edges, respectively, the loss of symmetry occurred at similar pole-to-pole distances. Indeed, for a straight line of thickness  $8 \mu\text{m}$  generating a symmetric structure, poles are  $\sim 38 \mu\text{m}$  apart, i.e., only 10% more than in a sperm-generated spindle. For lines of thickness  $13 \mu\text{m}$ , the distance between the poles would have to be  $\sim 43 \mu\text{m}$ , but the 2-fold symmetric interaction is unstable at this distance. On round spots, the loss of 2-fold symmetry occurred for diameters of  $\sim 24 \mu\text{m}$ , corresponding to a similar pole-to-pole distance of  $\sim 44 \mu\text{m}$  (Figure 3C). In other words, a pole-to-pole distance of  $\sim 43/44 \mu\text{m}$  is the upper range beyond which the bipolar symmetry is broken.

This transition to asymmetric structures is remarkable and difficult to explain because it may involve various factors that are shifted out of their normal equilibrium by the unusual chromatin width. For instance, growing microtubule plus ends may be pushing more on the chromatin or fast plus-ended chromokinesins may be more apt to transport microtubules away from the chromatin. Indeed, the magnitude of these effects is expected to increase with the width of the chromatin line. The transition is independent of dynein-mediated pole formation, since it occurs also in the presence of p50.

Most likely, microtubule antiparallel interactions dependent on the motor Eg5 weaken as the pole-to-pole distance increases, leading to a loss of symmetry when the chromatin is too wide. The results of hexylene glycol addition support this option: by increasing the microtubule length, it allowed spindles to accommodate a wider chromatin mass. Interestingly, the asymmetric structures on wide lines (Movie S5) are notably distinct from the phenotype observed in the presence of monastrol (Movie S7). Hence Eg5 must still play a role in the organization of the asymmetric structures, perhaps by bridging parallel microtubules. In

addition, the asymmetric structures are clearly dynamic. They are subject to a poleward tubulin flux that is comparable in direction and magnitude to that of bipolar spindles (Miyamoto et al., 2004). They even occasionally flip around the chromatin lines (Movie S5). Thus the asymmetric structures as well as the butterfly motifs (Figure 6F) are aberrant steady states that the cytoskeletal system produces under unusual chromatin configurations. They can be quite useful, however, because they provide critical tests for any mathematical models of the system.

Besides the asymmetric transition, dimensions associated with the different forces at work during mitosis were characterized. They are specific to *X. laevis* eggs and will be different in other species where the cytoplasmic factors have different activities. For example, we expect them to be reduced in the related but smaller frog *X. tropicalis* (Brown et al., 2007), but it will be interesting to see if their hierarchy is conserved. Our results on the effects of chromatin size on the length of the spindle are also coherent with previous observations. For example, using *X. tropicalis* sperms in a *X. laevis* extract or vice versa only changed spindle length by 10% (Brown et al., 2007; Wühr et al., 2008). Similarly, *X. laevis* spindles are able to fuse and form spindles that are 10% longer (Gatlin et al., 2009). In these experiments as well as in vivo, chromosomes are mobile. In addition, kinetochores and centrosomes are present, which can make spindles more robust. These effects will need to be studied to fully understand why spindles are resilient to loading.

The spindle arrays allowed us to change the amount of DNA and the geometry of chromatin, and thus probe the limits beyond which a proper bipolar architecture could not be formed. We initially used 0.5 pg of DNA per bead to match the physiological load of *X. laevis* spindles. Indeed, a typical spot of  $\sim 13$  beads (such as the one shown on Movie S4) then contained  $\sim 6.5$  pg of DNA, which roughly corresponds to a meiotic two load or half a mitotic load (the haploid genome of *X. laevis* weighs 3.2 pg; Thiébaud and Fischberg, 1977). However, changing the amount of DNA per bead only affected the system weakly (Figure 2), whereas changing the number of beads had a direct effect in all the tested configurations. A simple explanation of these results is that the surface of chromatin exposed to the extract is a more important factor than the total chromatin mass. Indeed, chromatin triggers microtubule assembly via enzymatic activities (Athale et al., 2008) and the cascade of reactions starts at the chromatin surface. We expect similarly that the surface area of chromosomes limit their signaling capacity in the cytoplasm.

This means that the spindle capacity in the bead assay is better expressed in number of beads rather than in mass of DNA. Indeed, with circular spots, spindles failed to form below approximately four beads and became multipolar for a diameter larger than  $\sim 20 \mu\text{m}$ , corresponding to a maximum of  $\sim 30$  beads. In the linear configuration, the maximum limits were  $\sim 10 \mu\text{m}$  for the width and  $\sim 30 \mu\text{m}$  for the length, roughly corresponding to the same area and thus the same average number of beads. The transition to multipolarity observed above these limits can be understood if one considers that microtubules have a characteristic length  $M$  set by the state of the cytoplasm. It is geometrically not possible to cover a patch larger than  $\sim M$  using two circles of size  $M$ . In other words, two microtubule asters are not

sufficient to cover the entire chromatin, if it is dispersed over a size larger than  $\sim M$ . There are two solutions to this geometrical puzzle: (1) the chromatin is covered by more than two circles. This is the result we obtained, corresponding to multipolar structures. (2) Only one spindle forms, but some chromatin is bare. This corresponds to the result observed by Gaetz et al. (2006). To investigate what disparity between the two assays may cause the discrepancy, we first used cycled extracts instead of CSF-arrested extracts, but the results were similar (data not shown). Second, we tested different amounts of DNA/bead, also without notable difference (data not shown). Fortuitously, after unusually long incubations, we sometimes observed only one spindle per line (Figure S6). This shows that the proximity of the glass in our assay does not prevent this phenotype. It further indicates that a single spindle may be produced when the extract is not fully potent. It is indeed possible that the rate of new microtubule generation by chromatin was lower in Gaetz et al., (2006) because the chromatin lines were thinner and/or because the incubation times in the chamber were longer. In both studies, however, the geometry of the chromatin cannot be handled by the microtubules that are not functionally organized: either some of the chromatin is “abandoned” or the overall symmetry is improper for bipolar division.

Can a spindle avoid this constraint altogether to handle more DNA? The answer is yes, and there are actually two ways to do this. The first one is to scale the entire structure up (increase  $M$ ). A bigger spindle with longer microtubules can embrace more chromatin. The second solution is less trivial and involves removing spindle poles. Adding p50 to inhibit dynein activity can do this. The structures produced on thin chromatin lines were neatly organized (Figure 4E). All bundles of microtubules were aligned perpendicularly to the chromatin line (Figure 4G). Therefore, in principle, chromosome segregation could proceed normally. In fact, chromosome segregation is observed with sperm heads in *X. laevis* egg in the presence of vanadate (Desai et al., 1998), anti-dynein antibodies (Gehmlich et al., 2004), or p50 (data not shown), with unfocused poles in all cases. In the absence of pole-forming agents such as dynein, increasing the length of the chromatin line did not disrupt the symmetric microtubule organization, which may thus accommodate a high quantity of DNA.

In practice, there are of course limitations imposed by cell size and other unknown factors, but all other things being equal, unfocused spindles in *X. laevis* egg extracts can handle more chromatin than focused ones. Remarkably, this may shed light on the difference of spindle architectures in higher (seeded) plants and animals. The spindles in seeded plants functionally segregate their sister chromatids without poles, centrosomes (Bornens and Azimzadeh, 2007), and dynein (Wickstead and Gull, 2007). They are naturally unfocused and similar to those obtained in *X. laevis* egg extracts by addition of p50. It could be that the unfocused spindle architecture allows plants to carry more DNA. Some plants indeed contain up to 260 pg of DNA per cell, about 40 times the amount present in *X. laevis*.

Spindle arrays routinely produce  $\sim 10,000$  spindles per  $\text{cm}^2$  and are compatible with further microfluidic constructions. It should therefore be possible to study the molecular players involved in spindle assembly systematically and precisely in the

future. It may as well be easier to measure the forces responsible for spindle formation when the DNA is immobilized. The possibility of imaging spindle assembly in *X. laevis* egg extracts from beginning to end is also an exciting stride forward.

## EXPERIMENTAL PROCEDURES

### *X. laevis* Egg Extract Preparation

*X. laevis* egg extracts were prepared as described previously (Hannak and Heald, 2006; Murray and Kirschner, 1989).

### Preparation of Chromatin Beads

YEp24 plasmid (New England Biolabs) was double digested with SmaI and BamHI. A first step of DNA biotinylation by fill-in reaction using biotin-dUTP and biotin-dATP was done as described (Hannak and Heald, 2006). Following the supplier's information, 2.3 or 0.5 pg/bead of the biotinylated DNA was bound to Dynal M-280 beads (Invitrogen). The immobilized DNA was further digested using NcoI. A second biotinylation step was performed using the same conditions. Chromatinization was done as described (Hannak and Heald, 2006), except that the DNA/bead incubation time with interphasic extract was reduced to 90 min and that four times more extract was used per bead with 2.3 pg of DNA (Figure 2) to avoid saturation of the reaction.

### Mask Design and Lithography

The masks were designed in CleWin (WieWeb) and produced by Delta Mask VDF. The silicon wafers were coated with  $^1\text{H}, ^1\text{H}, ^2\text{H}, ^2\text{H}$ -perfluorodecyltrichlorosilane solution (ABCR) before use.

### PDMS Incubation Chambers, Stamps, and Target Surfaces

Polydimethylsiloxane (PDMS) prepolymer and curing agent (Sylgard 184 kit; Dow Corning) were mixed in a 10:1 ratio. Mixture was poured onto hexagonal Teflon pieces (overall size was  $10 \times 5 \times 0.7$  mm) for chamber or onto silicon wafer for stamp preparation. Mixture was degassed under vacuum for 1 hr and cured at  $65^\circ\text{C}$  overnight. The chambers were cut individually and inlet and outlet were made on opposite side of the chamber using a needle with blunt gauge. The PDMS replica obtained from the silicon wafer was cut out according to the patterns. The stamps were on average  $5 \times 5$  mm. Target surfaces were prepared by coating clean, 30 mm round #1 coverslips (Menzel GmbH) with  $30 \mu\text{l}$  of PDMS mixture using a custom-built spin coater (EMBLCB-151D). The coverslips were then cured at  $65^\circ\text{C}$  overnight.

### Microcontact Printing

The stamps and target surfaces were activated by plasma treatment for 15 s (150 W; PlasmaPrep2; Gala Gabler Instrumente GmbH). The stamps were incubated in (3-aminopropyl) triethoxysilane (APTS; Sigma) solution (95% absolute ethanol, 3%  $\text{H}_2\text{O}$ , and 2% APTS) for 45 min and the target surfaces in (3-Glycidyl-oxypropyl) trimethoxysilane (Sigma) for 65 min. The stamps were rinsed once with absolute ethanol and twice with deionized water. They were dried on all sides, except for the patterned side, incubated in  $1 \text{ mg ml}^{-1}$  biotinylated BSA (Sigma) for 20 min at  $4^\circ\text{C}$ , and rinsed with water. The target surfaces were rinsed with acetone. For microcontact printing, both stamps and target surfaces were blown dry under pure nitrogen flow. Each stamp was carefully placed, patterned side down, in contact with the target surface for 30 min. The stamps were then removed and discarded. The printed surfaces were passivated with  $2.5 \text{ mg ml}^{-1}$  mPEG-NHS (Nanocs Inc) at  $4^\circ\text{C}$  for 60 min and with  $10 \text{ mg/ml}$  BSA (Sigma) at  $4^\circ\text{C}$  for 60 min and then washed in PBS. The surface was covered with  $50 \mu\text{l}$  of 2 M NaCl, 10 mM Tris-HCl (pH 7.6), and 1 mM EDTA solution containing  $5 \mu\text{l}$  streptavidin MyONE Dynabeads (Invitrogen) and incubated at  $4^\circ\text{C}$  for 2 hr. The printed surface was then washed with PBS and unbound beads were removed by gently pipetting up and down on the pattern region. The printed surfaces were stored in PBS at  $4^\circ\text{C}$  no longer than 1 week.

### Preparation of Reaction Chambers

Chromatinized DNA beads were resuspended in CSF-XB containing 0.5 M KCl and deposited over the printed area of the target surface. A weak magnet was

placed below the patterned surface to bring the chromatin DNA coated beads down to the streptavidin beads. The printed surface was then immersed in CSF-XB and unbound beads were removed by gently pipetting up and down over the patterned region using a pipette with a 1 ml tip. The surface was retrieved from the CSF-XB and dried with a filter paper, while keeping immersed the patterned surface containing the chromatin beads, which was kept wet. A PDMS microincubation chamber was placed above the printed area. A slight pressure on the chamber was sufficient to promote a good seal with the surface. The incubation chamber of volume V was then flushed with 2 V of CSF-XB. From this step on, the chamber was kept on ice until microscopy. It was first filled with a volume V of mitotic extract and just before imaging with a volume V of mitotic extract containing 24 mg/ml cyclin B  $\Delta$ 90 (Glotzer et al., 1991), 2.5  $\mu$ M Cy3-labeled tubulin, and 1  $\mu$ g/ml Hoechst dye (Invitrogen).

### Microscopy and Image Analysis

Microscopy was performed on a scanning fluorescence confocal microscope (LSM-Live 5 and LSM-Meta 510; Zeiss). The Zeiss LSM software was used for the image acquisition. A custom chamber (EMBL workshop) and cooling unit (Unichiller CC1; Hubert) were used to maintain a stable temperature of 20°C during the experiments. The length, width, and angles were measured using ImageJ (Wayne Rasband, National Institutes of Health).

The angles on round chromatin bead clusters were measured between an arbitrary vertical line and the axis of each bipolar spindle. For linear chromatin bead clusters the angles were measured between each DNA longest axis and the axis of its associated bipolar spindle. Analyses were performed in Matlab (The MathWorks), with custom macros available upon request. For Figure 2, two investigators identified the spindle poles independently with mouse clicks. C.P. reported a DNA-induced length increase of 10.8% from 30.60 to 33.31  $\mu$ m and F.N. an increase of 11.1% from 31.77 to 35.30  $\mu$ m. For Figure 3, fluorescence intensities were automatically analyzed and the beads were counted with similar results by three independent investigators.

### SUPPLEMENTAL DATA

Supplemental Data contain six figures, seven movies, and a video summary and can be found with this article online at [http://www.cell.com/supplemental/S0092-8674\(09\)00630-8](http://www.cell.com/supplemental/S0092-8674(09)00630-8).

### ACKNOWLEDGMENTS

A.D. and C.P. performed the experiments. M.M.C. established the chromatin patterning technique. M.L. developed the microfluidic chambers. M.M.C. obtained the initial results with M.L. J.S. and colleagues advised with micro-fabrication and offered access to the necessary facilities. E.K. contributed expertise with *X. laevis* egg extracts and bead assays and helped supervise the project. F.N. wrote the Matlab functions and analyzed the results with A.D. and C.P. He conceived and directed the research. F.N., A.D., and C.P. wrote the article with help from E.K. and M.L.

We thank C. Roduit, M. Kaksonen, R. Loughlin, T. Surrey, and J. Ward for critically reading the manuscript and Z. Gueroui for discussions. We used the Advanced Light Microscopy Facility and the animal facility at the European Molecular Biology Laboratory. We thank K. Crnokic, M. Caudron, S. Kandels-Lewis, S. Ruf (egg extracts), J. Ulmer and A. Lindner (microcontact printing), A. Wünsche (image acquisition), S. Laffont, M. Etzrodt, and N. Charuttini for help with the assay development. This work was supported by EU contract LSHG-CT-2004-503568 ComBio, the Spanish ministry of education (M.M.C.), and EU-STREP active BioMics (A.D.). Research in the Nedelec lab is funded by the Center for Modeling and Simulation in the Biosciences (<http://www.bioms.de>), the Volkswagenstiftung, and Human Frontier Science Program grant RGY84.

Received: November 24, 2008

Revised: March 9, 2009

Accepted: May 12, 2009

Published: August 6, 2009

### REFERENCES

- Antonio, C., Ferby, I., Wilhelm, H., Jones, M., Karsenti, E., Nebreda, A.R., and Vernos, I. (2000). Xkid, a chromokinesin required for chromosome alignment on the metaphase plate. *Cell* 102, 425–435.
- Athale, C.A., Dinarina, A., Mora-Coral, M., Pugieux, C., Nedelec, F., and Karsenti, E. (2008). Regulation of microtubule dynamics by reaction cascades around chromosomes. *Science* 322, 1243–1247.
- Bird, A.W., and Hyman, A.A. (2008). Building a spindle of the correct length in human cells requires the interaction between TPX2 and Aurora A. *J. Cell Biol.* 182, 289–300.
- Bornens, M., and Azimzadeh, J. (2007). Origin and evolution of the centrosome. *Adv. Exp. Med. Biol.* 607, 119–129.
- Bringmann, H., Skiniotis, G., Spilker, A., Kandels-Lewis, S., Vernos, I., and Surrey, T. (2004). A kinesin-like motor inhibits microtubule dynamic instability. *Science* 303, 1519–1522.
- Brown, K.S., Blower, M.D., Maresca, T.J., Grammer, T.C., Harland, R.M., and Heald, R. (2007). *Xenopus tropicalis* egg extracts provide insight into scaling of the mitotic spindle. *J. Cell Biol.* 176, 765–770.
- Burbank, K.S., Mitchison, T.J., and Fisher, D.S. (2007). Slide-and-cluster models for spindle assembly. *Curr. Biol.* 17, 1373–1383.
- Clausen, T., and Ribbeck, K. (2007). Self-organization of anastral spindles by synergy of dynamic instability, autocatalytic microtubule production, and a spatial signaling gradient. *PLoS ONE* 2, e244.
- Desai, A., and Mitchison, T. (1997). Microtubule polymerization dynamics. *Annu. Rev. Cell Dev. Biol.* 13, 83–117.
- Desai, A., Maddox, P.S., Mitchison, T.J., and Salmon, E.D. (1998). Anaphase A chromosome movement and poleward spindle microtubule flux occur at similar rates in *Xenopus* extract spindles. *J. Cell Biol.* 141, 703–713.
- Dogterom, M., Félix, M.A., Guet, C.C., and Leibler, S. (1996). Influence of M-phase chromatin on the anisotropy of microtubule asters. *J. Cell Biol.* 133, 125–140.
- Echeverri, C.J., Paschal, B.M., Vaughan, K.T., and Vellee, R.B. (1996). Molecular characterization of the 50-kD subunit of dynactin reveals function for the complex in chromosome alignment and spindle organization during mitosis. *J. Cell Biol.* 132, 617–633.
- Gaetz, J., Gueroui, Z., Libchaber, A., and Kapoor, T.M. (2006). Examining how the spatial organization of chromatin signals influences metaphase spindle assembly. *Nat. Cell Biol.* 8, 924–932.
- Gatlín, J.C., Matov, A., Groen, A.C., Needleman, D.J., Maresca, T.J., Danuser, G., Mitchison, T.J., and Salmon, E.D. (2009). Spindle fusion requires Dynein-mediated sliding of oppositely oriented microtubules. *Curr. Biol.* 19, 287–296.
- Gehmlich, K., Haren, L., and Merdes, A. (2004). Cyclin B degradation leads to NuMA release from dynein/dynactin and from spindle poles. *EMBO Rep.* 5, 97–103.
- Glotzer, M., Murray, A.W., and Kirschner, M.W. (1991). Cyclin is degraded by the ubiquitin pathway. *Nature* 349, 132–138.
- Goshima, G., Mayer, M., Zhang, N., Stuurman, N., and Vale, R.D. (2008). Augmin: a protein complex required for centrosome-independent microtubule generation within the spindle. *J. Cell Biol.* 181, 421–429.
- Hannak, E., and Heald, R. (2006). Investigating mitotic spindle assembly and function in vitro using *Xenopus laevis* egg extracts. *Nat. Protoc.* 1, 2305–2314.
- Heald, R., Tournebise, R., Blank, T., Sandaltzopoulos, R., Becker, P., Hyman, A., and Karsenti, E. (1996). Self-organization of microtubules into bipolar spindles around artificial chromosomes in *Xenopus* egg extracts. *Nature* 382, 420–425.
- Kapitein, L.C., Kwok, B.H., Weinger, J.S., Schmidt, C.F., Kapoor, T.M., and Peterman, E.J. (2008). Microtubule cross-linking triggers the directional motility of kinesin-5. *J. Cell Biol.* 182, 421–428.
- Karsenti, E., Newport, J., and Kirschner, M. (1984). Respective roles of centrosomes and chromatin in the conversion of microtubule arrays from interphase to metaphase. *J. Cell Biol.* 99, 47s–54s.

- Khodjakov, A., Cole, R.W., Oakley, B.R., and Rieder, C.L. (2000). Centrosome-independent mitotic spindle formation in vertebrates. *Curr. Biol.* *10*, 59–67.
- Lloyd, C., and Chan, J. (2006). Not so divided: the common basis of plant and animal cell division. *Nat. Rev. Mol. Cell Biol.* *7*, 147–152.
- Mahoney, N.M., Goshima, G., Douglass, A., and Vale, R. (2006). Making microtubules and mitotic spindles in cells without functional centrosomes. *Curr. Biol.* *16*, 564–569.
- Maresca, T.J., and Heald, R. (2006). Methods for studying spindle assembly and chromosome condensation in *Xenopus* egg extracts. *Methods Mol. Biol.* *322*, 459–474.
- Matthies, H.J., McDonald, H.B., Goldstein, L.S., and Theurkauf, W.E. (1996). Anastral meiotic spindle morphogenesis: role of the non-claret disjunctional kinesin-like protein. *J. Cell Biol.* *134*, 455–464.
- Mayer, T.U., Kapoor, T.M., Haggarty, S.J., King, R.W., Schreiber, S.L., and Mitchison, T.J. (1999). Small molecule inhibitor of mitotic spindle bipolarity identified in a phenotype-based screen. *Science* *286*, 971–974.
- Mitchison, T.J., Maddox, P., Gaetz, J., Groen, A., Shirasu, M., Desai, A., Salmon, E.D., and Kapoor, T.M. (2005). Roles of polymerization dynamics, opposed motors, and a tensile element in governing the length of *Xenopus* extract meiotic spindles. *Mol. Biol. Cell* *16*, 3064–3076.
- Miyamoto, D.T., Perlman, Z.E., Burbank, K.S., Groen, A.C., and Mitchison, T.J. (2004). The kinesin Eg5 drives poleward microtubule flux in *Xenopus laevis* egg extract spindles. *J. Cell Biol.* *167*, 813–818.
- Murray, A.W., and Kirschner, M.W. (1989). Cyclin synthesis drives the early embryonic cell cycle. *Nature* *339*, 275–280.
- Schuh, M., and Ellenberg, J. (2007). Self-organization of MTOCs replaces centrosome function during acentrosomal spindle assembly in live mouse oocytes. *Cell* *130*, 484–498.
- Thiébaud, C.H., and Fischberg, M. (1977). DNA content in the genus *Xenopus*. *Chromosoma* *59*, 253–257.
- Tokai-Nishizumi, N., Ohsugi, M., Suzuki, E., and Yamamoto, T. (2005). The chromokinesin Kid is required for maintenance of proper metaphase spindle size. *Mol. Biol. Cell* *16*, 5455–5463.
- Valentine, M.T., Fordyce, P.M., Krzysiak, T.C., Gilbert, S.P., and Block, S.M. (2006). Individual dimers of the mitotic kinesin motor Eg5 step processively and support substantial loads in vitro. *Nat. Cell Biol.* *8*, 470–476.
- Walczak, C.E., and Heald, R. (2008). Mechanisms of mitotic spindle assembly and function. *Int. Rev. Cytol.* *265*, 111–158.
- Walczak, C.E., Vernos, I., Mitchison, T.J., Karsenti, E., and Heald, R. (1998). A model for the proposed roles of different microtubule-based motor proteins in establishing spindle bipolarity. *Curr. Biol.* *8*, 903–913.
- Waterman-Storer, C.M., Desai, A., Bulinski, J.C., and Salmon, E.D. (1998). Fluorescent speckle microscopy, a method to visualize the dynamics of protein assemblies in living cells. *Curr. Biol.* *8*, 1227–1230.
- Wickstead, B., and Gull, K. (2007). Dyneins across eukaryotes: a comparative genomic analysis. *Traffic* *8*, 1708–1721.
- Winey, M., Mamay, C.L., O'Toole, E.T., Mastronarde, D.N., Giddings, T.H., McDonald, K.L., and McIntosh, J.R. (1995). Three-dimensional ultrastructural analysis of the *Saccharomyces cerevisiae* mitotic spindle. *J. Cell Biol.* *129*, 1601–1615.
- Wittmann, T., Hyman, A., and Desai, A. (2001). The spindle: a dynamic assembly of microtubules and motors. *Nat. Cell Biol.* *3*, E28–E34.
- Wühr, M., Chen, Y., Dumont, S., Groen, A.C., Needleman, D.J., Salic, A., and Mitchison, T.J. (2008). Evidence for an upper limit to mitotic spindle length. *Curr. Biol.* *18*, 1256–1261.